Dendritic spines linearize the summation of excitatory potentials

Roberto Araya, Kenneth B. Eisenthal*, and Rafael Yuste*

Howard Hughes Medical Institute and Departments of Biological Sciences and Chemistry, Columbia University, New York, NY 10027

Contributed by Kenneth B. Eisenthal, October 18, 2006 (sent for review July 27, 2006)

In mammalian cortex, most excitatory inputs occur on dendritic spines, avoiding dendritic shafts. Although spines biochemically isolate inputs, nonspiny neurons can also implement biochemical compartmentalization; so, it is possible that spines have an additional function. We have recently shown that the spine neck can filter membrane potentials going into and out of the spine. To investigate the potential function of this electrical filtering, we used two-photon uncaging of glutamate and compared the integration of electrical signals in spines vs. dendritic shafts from basal dendrites of mouse layer 5 pyramidal neurons. Uncaging potentials onto spines summed linearly, whereas potentials on dendritic shafts reduced each other's effect. Linear integration of spines was maintained regardless of the amplitude of the response, distance between spines (as close as <2 μm), distance of the spines to the soma, dendritic diameter, or spine neck length. Our findings indicate that spines serve as electrical isolators to prevent input interaction, and thus generate a linear arithmetic of excitatory inputs. Linear integration could be an essential feature of cortical and other spine-laden circuits.

second harmonic | pyramidal cell | glutamate uncaging | two-photon

In neocortex and many other brain areas, most excitatory inputs terminate on dendritic spines (1); so, spines must therefore likely be of major importance for the functioning of neural circuits (2). Spines can compartmentalize calcium (3), partly because their peculiar morphologies, with a small head separated from the dendrite by a slender neck, enable the biochemical isolation between inputs (4–6). This compartmentalization is thought to underlie input-specific forms of synaptic plasticity, such as long-term potentiation (7–9).

Theoretical work spanning several decades has suggested that spines are ideally poised to play a major role in altering the electrical properties of synaptic inputs (2, 10–14). Indeed, recent work has called into question the view that the sole function of spines is one of biochemical compartmentalization. First, nonspiny neurons can compartmentalize calcium with as good a degree of biochemical isolation between inputs as spiny cells (15, 16). Also, by using glutamate uncaging and second harmonic measurements of membrane potential on spines of layer 5 pyramidal neurons, we have demonstrated that the spine neck filters membrane potentials (17). The filtering was bidirectional, i.e., both spine potentials transmitted to the dendrite and dendritic potentials transmitted to the spine were strongly attenuated. This implies that spines could isolate inputs electrically, an idea previously suggested based on theoretical calculations (11, 12, 18). More generally, passive cable models predict that inputs onto dendrites will shunt each other if they are close (19, 20). Therefore, dendritic spines could provide an electrically isolated postsynaptic region to prevent interaction between different excitatory inputs, resulting in a linear integration (21).

Consistent with these predictions, experiments using iontophoretic application of glutamate or synaptic activation of dendrites from hippocampal pyramidal cells demonstrated that summation of excitatory inputs is remarkably linear (22, 23). In addition, neocortical neurons integrate excitatory inputs linearly *in vitro* (24) and *in vivo* (25). Summation experiments using one-photon uncaging of glutamate or extracellular stimulation on neocortical pyramidal neurons have confirmed that excitatory inputs as close as 40 μm can sum linearly, although closer stimulation, or stimulation with stronger currents, generated local spikes (26–28). These studies did not examine input integration with a spatial resolution of single inputs, important because the predicted cable shunting would arise from interaction between very close, or neighboring, inputs. This problem has been solved by the recent introduction of two-photon uncaging of glutamate (29), made possible by the synthesis of a new generation of 4-methoxy-7-nitroindolinyl (MNI) chemical cages (30). With high numerical aperture objectives, the two-photon point spread function is comparable to the size of a typical spine head (31), and two-photon uncaging can be used to precisely activate glutamate receptors in a spatial region comparable to that activated physiologically by a single excitatory input. Indeed, recent two-photon glutamate uncaging experiments have explored dendritic summation, finding linearity of integration for inputs for regimes when several spines are activated (32, 33). At the same time, these studies did not explore the possibility that spines are necessary for linear integration.

In the present work, we pose the question whether, because the spine neck acts as an electrical filter (17), spines are the reason pyramidal neurons integrate linearly. For this purpose, we use two-photon uncaging of MNI-glutamate as an optical tool to generate a local depolarization in a desired position of the dendritic tree (spine or shaft locations) with a spatial resolution that allow us to differentiate between excitation at two shaft locations vs. excitation at two (or three) spine locations. We therefore examined input summation onto dendritic spines or shafts of neocortical neurons from mouse visual cortical slices and characterized the potential effect of interspine distance, distance from the soma, and spine neck length. Our experimental design was simple: uncage glutamate onto spines separately and then together, evaluate the summation of their combined effect by measuring the generated somatic depolarization, and compare these results with uncaging experiments in nonspiny regions of the dendritic shaft.

Our results demonstrate that uncaging events sum linearly ($\approx$100% of expected arithmetic sum) if they occur on spines, but they sum sublinearly, interfering with each other and resulting in an average $\approx$70% summation, if they occur on dendritic shafts. Linear summation is present even among immediately neighboring spines and is not affected by input size, interspine distance, distance to the soma, dendritic diameter, or spine neck length. Our results confirm that the spines can electrically isolate excitatory inputs and are determinants in effecting a linear

Author contributions: R.A., K.B.E., and R.Y. designed research, analyzed data, and wrote the paper.

The authors declare no conflict of interest.

Abbreviations: EPSP, excitatory postsynaptic potential; MNI, 4-methoxy-7-nitroindolinyl.

*To whom correspondence may be addressed. E-mail: kbe1@columbia.edu or rmy5@columbia.edu.

NEUROSCIENCE

integration of input signals by the neuron. Thus, spines could serve to protect dendritic integration from changes in input resistance during synaptic transmission (11).

Results

Two-Photon Uncaging of MNI-Glutamate with Single-Spine Resolution. To compare the integration of synaptic inputs observed upon stimulation of dendritic spines vs. stimulation of dendritic shafts, we used two-photon uncaging of MNI-glutamate (29, 30) to activate spines and dendritic shafts located 15–125 μm away from the soma on basal dendrites from layer 5 pyramidal neurons of mouse V1 slices (17, 34). Neurons were patch clamped and filled with Alexa Fluor 488 for imaging (Fig. 1*A Left*), and basal dendrites were imaged at high magnification to select regions where several spines were located in the same focal plane (Fig. 1*A Right*). For each region studied, we obtained *z*-section stacks of images, and thus were able to identify the position of all spines in the area. By using these stacks, we discarded data sets in which out-of-focus spines could become accidentally stimulated by the uncaging laser.

We mimicked the synaptic activation of individual spines with two-photon uncaging of glutamate to achieve a local depolarization of the spine. The uncaging laser was focused immediately adjacent to the spine head (≈0.2 μm from the spine head edge), and somatic measurements of membrane potential were performed in current clamp. The gating of the laser generated small depolarizations at the soma ("uncaging potentials"), which were similar in amplitude to those observed spontaneously (0.97 ± 0.14 mV for uncaging potentials, $n = 26$ spines and 8 cells, vs. 0.86 ± 0.07 mV for spontaneous excitatory postsynaptic potentials (EPSPs), $n = 61$ events and 6 cells, P value = 0.45; t test; mean ± SEM for all measurements). As shown before (17), the functional region activated by glutamate uncaging was ≈1 μm in diameter, i.e., moving the uncaging laser spot ≥ 1.5 μm from the spine head did not generate an uncaging potential.

Linear Summation of Uncaging Potentials from Spines. We first measured the sum of two (or three) excitatory inputs on different spines, located at various distances from the soma (Fig. 1*B*). Five to 15 cycles of stimulation were performed. Each cycle included first the stimulation of each spine independently, with a 2-s interval, and second, the activation of two (or three) spines with a 5-ms interval between uncaging events (Fig. 1*C Upper*). To assess the effect of the uncaging events, the average peak amplitude and integral values caused by uncaging potentials were measured independently and then compared with the combined response (Fig. 1*C Upper*, red trace). Specifically, the percentage summation was calculated by comparing the peak membrane potential amplitude and area of the combined response with the expected sum of the individual events (Fig. 1*C Upper*, black trace). These results indicated that uncaging potentials onto spines summed linearly (two inputs: amplitude, 98.8 ± 1.9% of expected linear sum; area, 104.3 ± 3.6%; $n = 7$ pairs of spines; five cells; three inputs: amplitude, 107.4 ± 5% of expected linear sum; area, 103.4 ± 8%; $n = 4$ triplets; three cells). Across individual pairs or triplets of spines, summation ranged from ≈90% to 120%. Pooled data (including two and three spine stimulations) revealed that uncaging potentials in spines summed linearly (Fig. 2*C*; amplitude: 101.9 ± 2.4% of expected linear sum, $P = 0.43$; area: 104 ± 3.4%; $n = 7$ pairs of spines and $n = 4$ triplets of spines, $P = 0.28$).

Sublinear Summation of Uncaging Potentials from Dendritic Shafts. We next measured how two uncaging potentials from dendritic shafts were summed stimulating sites at 20 to 80 μm from the soma (Fig. 1 *B* and *C Lower*). The stimulation protocol was the same as the one used on spines: the laser beam was positioned immediately adjacent to the shaft (≈0.2 μm from the shaft edge),

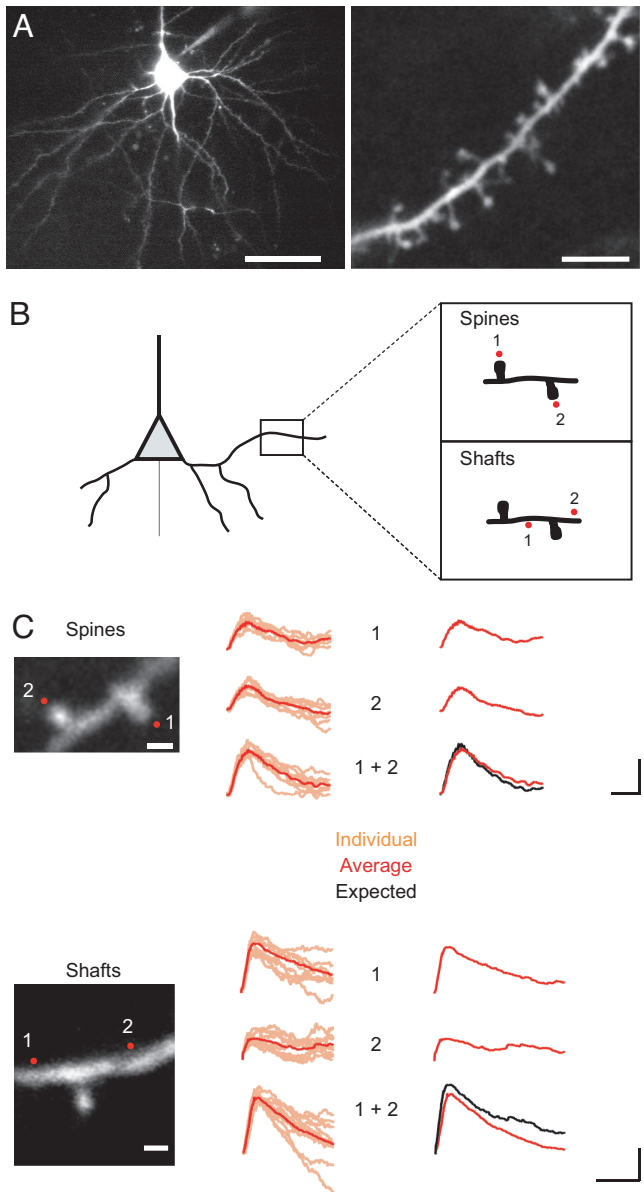

Fig. 1. Summation of uncaging potentials on spines and dendritic shafts. (*A*) (*Left*) Layer 5 pyramidal cell filled with Alexa Fluor 488. (Scale bar: 50 μm.) (*Right*) Representative basal dendrite selected for uncaging. (Scale bar: 5 μm.) (*B*) Protocol for testing summation. Red dots indicate the site of uncaging in spines or shaft locations. Uncaging was performed first at each spine or shaft location (1 or 2) and then in either both spines together or in both shaft locations (1 + 2). (*C*) (*Upper*) Summation in spines. (*Left*) Individual examples. (*Right*) Averages. Red traces correspond to an average of 10 depolarizations (orange traces) caused by uncaging over each of the two spines, and black traces correspond to the expected algebraic (linear) sum of the individual events of each spine. Note how the average response is close to expected. (Scale bar: 1 μm/2 mV/50 ms.) (*Lower*) Summation in shafts. Data are presented as in *B*. Note the sublinear summation. (Scale bars: 1 μm/1 mV/50 ms.)

and the somatic depolarizations caused by uncaging at one or two shaft locations were measured separately. To prevent overlap, locations along the shaft were separated by at least 2 μm. Uncaging of glutamate at different shaft locations along the basal dendrite generated small somatic depolarizations similar in amplitude (0.83 ± 0.11 mV, $n = 18$ locations and 7 cells) to those observed with uncaging events onto dendritic spines ($P = 0.47$). Again, the percentage linearity was calculated by measuring the peak amplitude and integral values of the combined response

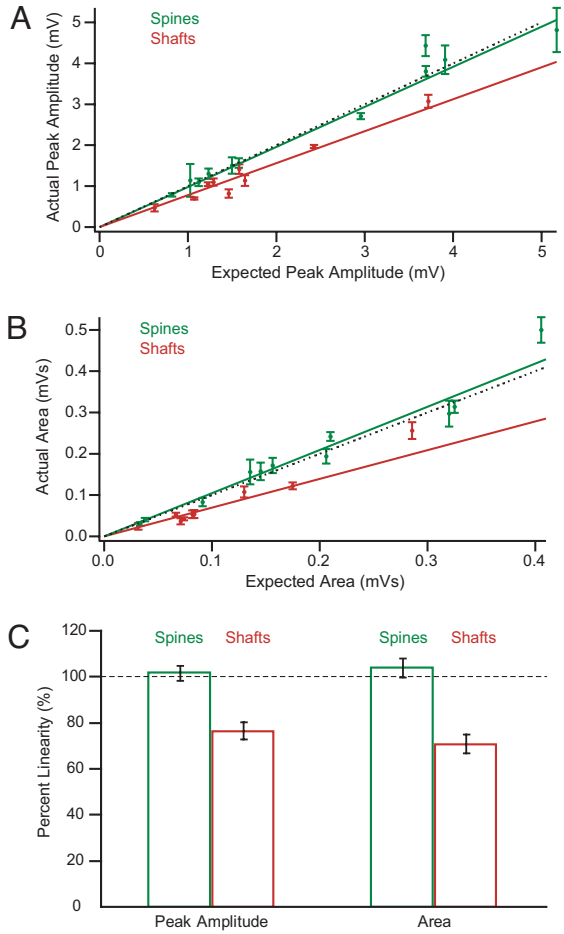

Fig. 2. Input summation is linear in spines and sublinear in shafts. Dependency of summation on uncaging potential strengths. (*A* and *B*) Plot of the actual vs. the expected peak amplitudes (*A*) and actual vs. the expected areas (*B*) from uncaging events in spines (green) or shafts (red) on basal dendrite of layer 5 pyramidal cell. Inputs onto spines sum linearly at small and large amplitudes, but inputs onto dendritic shafts sum sublinearly. The dotted line shows expected linear summation, and the solid lines are linear regression fits to the uncaging data ($P < 0.005$, Mann–Whitney comparing spines vs. shafts). (*C*) Summary of results. Linearity is expressed as the ratio of the peak amplitude or area of the combined event to the expected values, calculated by adding the two separate events. Data are presented as averages ± SEM.

over two shaft locations (Fig. 1*C Lower*; red trace) and comparing it with the expected sum of the individual events (Fig. 1*C Lower*, black trace). In contrast to the spines, uncaging potentials on two shaft locations demonstrated sublinear integration, i.e., the combined event was significantly *smaller* than the sum of individual events (Figs. 1*C Lower* and 2*C*; amplitude: 76.4 ± 3.6% of expected linear sum, $P < 0.005$; area: 70.8 ± 4.1%, $P < 0.005$, $n = 9$ experiments, pooled data). A sublinear response was present in every pair of locations examined, and the reduction in combined response could approach 50% of the expected value (Fig. 3). Our combined results thus indicated that uncaging events revealed a linear integration regime for the concurrent depolarization of spines, yet interacted in a sublinear manner for dendritic shafts.

Integration Is Independent of Input Size, Distance from Soma, Interspine and Intershaft Distances, Dendrite Diameter, and Spine Neck Length. To characterize the dependency of integration on input size, we plotted the actual vs. expected peak amplitude and area from uncaging events for all spines and shafts locations (Fig. 2). At both small and large amplitudes, inputs onto spines summed linearly, whereas inputs onto dendritic shafts summed sublinearly (Fig. 2*A*). Specifically, although spine integration had a slope of ≈1, integration on shafts had a slope significantly <1 (linear regression fits: spines, slope 0.97 ± 0.01; shafts, slope 0.78 ± 0.01; $P < 0.005$, Mann–Whitney analysis comparing spines vs. shafts). Similarly, analysis of the actual vs. expected areas (Fig. 2*B*) indicated that inputs onto spines summed with a slope of ≈1, whereas those on shafts had a lower slope, indicating interaction (spines: slope 1.04 ± 0.02; shafts: slope 0.69 ± 0.02; $P < 0.005$, Mann–Whitney).

Secondly, we determined whether interspine distance influenced input summation. We thus directly examined one of the predictions from cable models of dendrites, by which neighboring inputs would reduce each other's effect (19). The interspine distance between two spines was measured from the base of the first spine to the base of the second spine. For three spine experiments we measured the average distances between all spine pairs. Pooled data showed that the distance between activated spines had no discernible impact on the summation, even finding linearity in pairs of spines whose neck attachments were as close as 1.1 μm from each other (Fig. 3*A*; amplitude, $r = 0.46$, $P = 0.15$; area, $r = 0.18$, $P = 0.58$). Similarly, we did not observe any correlation between the summation and the distance between activated dendritic shafts (Fig. 3*A*; amplitude, $r = 0.1$, $P = 0.79$; area, $r = 0.46$, $P = 0.2$). In addition, we determined whether the distance of the activated spines or dendritic shafts to the soma influenced the degree of summation observed because the structure, size, and functional properties of spines can vary as a function of their location along the dendritic tree (35–37). Linear regression analyses indicated that integration of inputs onto spines or shafts was not affected by their distance from soma (Fig. 3*B*, spines: amplitude, $r = 0.24$, $P = 0.47$; area, $r = 0.5$, $P = 0.08$; shafts: amplitude, $r = 0.49$, $P = 0.18$; area, $r = 0.59$, $P = 0.09$).

We also examined whether the dendritic diameter correlated with the degree of summation observed in spines or shafts because the dendritic diameter can affect the degree of electrical isolation between spines (38). In the population of basal dendrites examined, dendrite diameter ranged from ≈0.6 to 1 μm in diameter, with an approximate average of 0.75 μm ($n = 20$ dendrite locations). In our pooled data, we found no correlation in the summation of spine or shaft uncaging potentials and dendritic diameter (spines: amplitude, $r = 0.3$, $P = 0.31$ and area, $r = 0.19$, $P = 0.56$; shaft: amplitude, $r = 0.29$, $P = 0.44$ and area, $r = 0.25$, $P = 0.5$).

Finally, we also examined whether the length of the spine neck affected input summation. Indeed, based on passive cable theory, one would expect a strong dependency between the spine neck length and the linearity of the summation because the neck resistance, and therefore the degree of electrical isolation between spines, should be proportional to the neck length. We tested this by examining the average spine neck length value of the studied spines in each experiment vs. the percent linearity (Fig. 3*C*). These analyses failed to show a significant modulation of input linearity by the neck length (amplitude, $r = 0.24$, $P = 0.47$; area, $r = 0.36$, $P = 0.26$). To further evaluate this possibility, we separated the experiments into three groups: short spines, which included spine pairs/triplets with spines that had only neck lengths of 0.2 μm; mixed spines, which included spines with short and long neck lengths; and long spines, with spines that had only neck lengths of at least 0.5 μm. In this analysis, although there was a small trend, we still did not observe any significant modulation of spine integration with neck length (short spines: amplitude, 98.78 ± 5.21%, $P = 0.83$ vs. 100% linearity; area, 95.36 ± 1.18%, $P = 0.06$, $n = 2$ experiments with 0.2/0.2- and 0.2/0.2-μm neck lengths; mixed spines: amplitude, 100.59 ± 2.33%, $P = 0.8$, area, 105.59 ± 3.87%, $P = 0.17$, $n = 7$; long

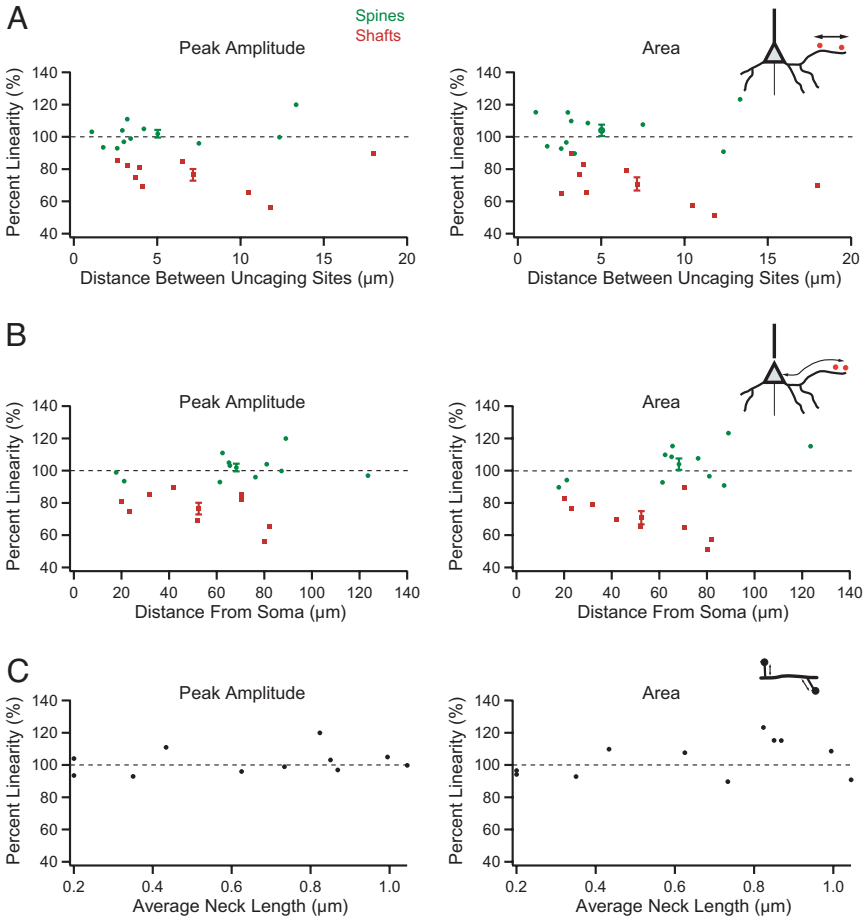

Fig. 3. Spine linearity is not affected by interspine distance, distance to the soma, or neck length. Summation of uncaging potentials is not affected by the distance between uncaging stimuli (*A*), distance of those inputs from the soma (*B*), or the average neck length (*C*). Color circles represent the mean ± SEM percentage linearity of the experiments from each condition, positioned at average *x* axis value.

spines: amplitude, 109.9 ± 10.1%, $P = 0.5$, area, 107.08 ± 16.22%, $P = 0.73$, $n = 2$ with 1.0/0.8/0.67- and 1.2/1.07/0.85-μm neck length).

Discussion

In this work, we find that excitatory uncaging events activated at spines (as close as 1.1 μm) sum close to 100% linearity (102% of peak voltage amplitude and 104% of area), whereas inputs onto dendritic shafts sum sublinearly (76% of amplitude and 70% of area). This difference is significant, robust, and maintained across a large range of experimental variables. We interpret these results as consistent with the hypothesis that dendritic spines serve as electrical isolators that promote linear integration (11, 12, 18, 21).

Our interpretation of these results depends on several assumptions. The first one is that the method used is an appropriate experimental approximation to examine input integration because we performed our measurements using an artificial means of stimulating the neuron, with two-photon uncaging of MNI-glutamate. Our primary goal was to use this approach as a tool to create localized excitatory conductances and to spatially probe the dendritic tree, rather than as a true substitute for physiological release, because the spatiotemporal dynamics of the glutamate uncaging pulse are different from those achieved at the synaptic cleft during normal synaptic transmission. Because of this, physiological EPSPs occurring at the head of the spine could lead to very different results. However, unitary EPSPs from layer 5 pyramidal neurons are similar in amplitude to our uncaging events (see figure 7 in ref. 39). In addition, linear summation of EPSPs (presumably activating spines) has been found in CA1 (23) and neocortical pyramidal neurons *in vitro* (24, 27) and *in vivo* (25).

Another assumption we make is that there is no significant spread of the uncaging glutamate to neighboring spines of the recorded cell. Although the uncaging point spread function is ≈1 μm in lateral resolution, it is likely to be ≈2 μm in z, and it is conceivable that spines located out of focus could be also stimulated. We controlled for this by performing z-stacks of every imaged dendrite and did not use any data when out-of-focus spines were located within 3 μm of the stimulated spine. Moreover, we observed no trend in spine linearity or shaft sublinearity as a function of distance between uncaging events (Fig. 3), effectively ruling out a stimulation overlap problem.

What are the biophysical mechanisms that underlie these two different summation regimes in spines and dendritic shafts? In principle, our data could be explained by passive mechanisms, intrinsic to the cable structure of these neurons, or by mechanisms involving active conductances. In the passive case, sublinear summation could be generated by a reduction of the driving force by the joint stimuli or by a shunting of voltage by the open synaptic conductances.

We address first the potential mechanisms that could explain the dendritic shaft results. How do uncaging potentials on the shaft integrate sublinearly, whereas similar depolarizations, when they enter the same dendritic shafts through the spine neck, sum linearly? Given that a key difference between both

cases is the location of activated glutamate receptors, as a potential solution to this paradox, we would propose that the opening of glutamate receptors (or secondary conductances activated by them or by the uncaged glutamate) in the shaft are shunting potentials locally. Thus, open shaft glutamate receptors would shunt shaft potentials, but not the similar-sized potentials injected by the spine, which would propagate without attenuation, because the shaft receptors will then be closed. This local shunting mechanism could explain the shaft sublinearity and the linear integration of spine potentials. A driving force reduction cannot explain these two different results, and we would rule it out because of the discrepancy between the small reduction in driving force that the 1- to 2-mV uncaging potentials could generate in the shaft, as compared with the large (≈70%) sublinearity measured. One prediction from our shaft-shunting model would be that shaft stimulation could shunt a spine stimulation. Consistent with this, in one preliminary experiment, we have found that the activation of one spine and shaft location results in a sublinear summation (77% in peak amplitude, 83% in area, $n = 1/1$). Finally, this local shunt scenario would agree with our recent findings that the spine neck filters membrane potentials (17), as if the neck were protecting the dendritic shaft (and other spines) from shunting effects, and potentially large potentials, of spine synaptic conductances.

In the case of the spine integration, the linearity could be ensured by the protective effect of spine necks to minimize shunting interactions. Nevertheless, if this were the only mechanism, one would expect a significant modulation of the spine linearity by spine neck length, something that we do not observe. Specifically, short-neck spines should interact more than long-neck ones (17). Although we cannot rule out that further experiments could reveal a neck effect, it is possible that active conductances are at work in the spine contributing to generate the linear summation. Indeed, our past results in CA1 cells (22, 23) revealed that a balance of active conductances was responsible for normalizing linear integration in CA1 cells (an ''active linearity''). In any case, it is difficult to meaningfully discuss the mechanisms operating on the spine given our ignorance about the exact value of the uncaging potential (or synaptic EPSP) at the head of the spine, because the mechanisms operating could be voltage dependent. The recent introduction of second harmonic measurements of membrane potential in spines could help provide this key missing measurement (40).

How general are these results? Although we have only explored basal spines at particular distances (most of them at 20–80 μm) from the soma, the locations of the examined spines cover the regions of highest spine density in pyramidal neurons (34, 41), and basal dendrites can host the majority of the spines of pyramidal cells (42). With respect to other cell types besides mouse layer 5 neurons, linear or near-linear summation of EPSPs has been also documented in rat hippocampal pyramidal neurons (22, 23), rat neocortical layer 2/3 and layer 5 cells *in vitro* (24, 27) and *in vivo* (25), and even rat Purkinje cells *in vitro* (43). Because all of these neurons share spine-laden dendrites, we would extend our interpretation to spiny cells more generally, proposing that the reason these neurons integrate linearly is precisely because their inputs are mediated by spines.

Our results have implications for the function of dendritic spines and cortical circuits. The difference in input integration in spines vs. dendritic shafts indicates that dendritic spines serve not merely as biochemical compartments, but have an electrical function as well, as proposed by theoretical studies (2, 11, 12, 18, 44). Our data are consistent with this idea, extending the previous demonstration that the spine neck can filter membrane potentials (17), and can also provide a functional logic for this filtering: spines would serve to electrically isolate inputs (also reducing their voltage effect in the dendrite) and prevent their interaction. This could explain why excitatory axons do not terminate on dendritic shafts. Finally, given how prevalent spines are in cortical circuits, the uncovering of their role in linearizing summation suggests that linear integration could be of the essence for cortical processing (21). A linear integration agrees with the excitatory connectivity in neocortex that is composed of a very distributed matrix with relatively few synaptic contacts between excitatory neurons (45). If the logic of the cortex is to distribute the information to a large number of postsynaptic cells as in a ''neuronal democracy,'' it is only fitting that those neurons integrate inputs linearly (21). Thus, the pyramidal neuron might be computationally simple, and its apparently complex dendritic morphology could paradoxically serve to linearize its input integration.

Materials and Methods

Slice Preparation. All animal handling and experimentation was done according to the National Institutes of Health and local Institutional Animal Care and Use Committee guidelines. Coronal slices of visual cortex that were 300 μm thick were prepared from P14–15 C57BL/6 mice as described (15). Animals were anesthetized with ketamine-xylazine (50 and 10 mg·kg^{-1}).

Imaging and Electrophysiology. All experiments were performed at 37°C. Neurons were filled with 200 μM Alexa Fluor 488 (Molecular Probes, Eugene, OR) through the recording pipette. Pipette solution contained 135 mM KMeSO4, 10 mM KCl, 5 mM NaCl, 10 mM Hepes, 2.5 mM Mg-ATP, 0.3 mM GTP (pH 7.3). After cells were fully loaded with dye (15–30 m after break in), dendritic location or spines were selected for imaging and uncaging. Imaging was done by using a custom-made, two-photon, laser-scanning microscope (46) consisting of a modified Fluoview (Olympus, Melville, NY) upright confocal microscope with a Ti:sapphire laser (Chameleon; Coherent, Santa Clara, CA). A ×60, 1.1 N.A. objective (Olympus) was used. Images were acquired at the highest digital zoom (a magnification of ×10). Distances from the soma and neck length were measured from the site of dendritic imaging to the location where the parent dendrite emerged from the soma and from the proximal edge of the spine head to the dendrite, respectively, with Image J (National Institutes of Health). Neck lengths apparently <0.2 μm were counted as 0.2 μm. Unless mentioned otherwise, two-sided Student t tests were used, and data are presented as mean ± SEM.

Two-Photon Uncaging of Glutamate. MNI-caged glutamate (2.5 mM; Tocris Cookson, Bristol, United Kingdom) was bath-applied, and a Dynamax peristaltic pump (Rainin Instruments, Woburn, MA) was used to control bath perfusion and to minimize total bath volume. Our two-photon microscope was controlled by software developed in-house (46), and imaging and uncaging were performed at 725 nm (Chameleon laser; Coherent). The laser was positioned at a distance of ≈0.2 μm from spine heads or dendritic shafts of layer 5 pyramidal neurons that were filled with 200 μM Alexa Fluor 488 through recording pipettes. Laser power was controlled by a Pockels cell (Quantum Technology, Lake Mary, FL) that was gated by square pulses (Master-8, A.M.P.I., Jerusalem, Israel). For uncaging, 4-ms laser pulses at 2-s intervals or sequential 4-ms pulses were used with 25–30 mW of power on the sample plane. Including the delay between the uncaging in spines or shafts in the analyses did not generate a significant difference in the percentage linearity of the peak amplitude (not shown). Similar results were obtained in test experiments with 2-ms uncaging pulses (data not shown). In addition, it should be noted that the uncaging potentials normally lasted 50–100 ms and were thus much larger than the 4-ms uncaging pulses. For imaging, 5–8 mW of laser power was used. Voltage deflections due to the glutamate uncaging (uncaging potentials) were recorded from the soma in whole-cell

current clamp at a resting potential of −65 mV using standard electrophysiology equipment and were analyzed off-line. Data were analyzed by custom-written software using MATLAB (MathWorks, Natick, MA) and Igor (WaveMetrics, Lake Oswego, OR).

We wondered whether the observed linear uncaging results could have been generated by changes in the electrical properties of the neurons being modified by our experimental manipulation. Specifically, our use of Alexa Fluor 488 could have compromised our measurements because K^+ channels can be blocked by free radicals generated after photodamage (47). Nevertheless, in our experiments with Alexa-filled cells, the action potential widths were comparable to those from non-Alexa-filled cells (data not shown). Furthermore, we observed linear summation regimes in spines with much smaller concentrations of Alexa (≈50 μM instead of 200 μM) or using calcium green-1 instead of Alexa Fluor 488 (data not shown). In addition, linear summation of EPSPs has been demonstrated in neurons that were not filled with any dye (see figure 7 in ref. 23).

We thank V. Nikolenko for help with the uncaging and A. Trevelyan and members of the laboratory for comments. This work was funded by the National Eye Institute, the Pew Program in Biomedical Sciences, and the New York STAR Center for High Resolution Imaging of Functional Neural Circuits. K.B.E. thanks the National Science Foundation for support.

1. Ramón y Cajal S (1888) *Rev Trimest Histol Norm Patterns* 1:1–10.
2. Shepherd G (1996) *J Neurophysiol* 75:2197–2210.
3. Yuste R, Denk W (1995) *Nature* 375:682–684.
4. Svoboda K, Tank DW, Denk W (1996) *Science* 272:716–719.
5. Majewska A, Tashiro A, Yuste R (2000) *J Neurosci* 20:8262–8268.
6. Yuste R, Majewska A, Holthoff K (2000) *Nat Neurosci* 3:653–659.
7. Wickens J (1988) *Prog Neurobiol* 31:507–528.
8. Koch C, Zador A (1993) *J Neurosci* 13:413–422.
9. Matsuzaki M, Honkura N, Ellis-Davies GC, Kasai H (2004) *Nature* 761–766.
10. Chang HT (1952) *Cold Spring Harbor Symp Quant Biol* 17:189–202.
11. Llinás R, Hillman DE (1969) in *Neurobiology of Cerebellar Evolution and Development*, ed Llinas R (Am Med Assoc Educat Res Found, Chicago), pp 43–73.
12. Jack JJB, Noble D, Tsien RW (1975) *Electric Current Flow in Excitable Cells* (Oxford Univ Press, London).
13. Rall W (1974) in *Studies in Neurophysiology*, ed Porter R (Cambridge Univ Press, Cambridge, United Kingdom), pp 203–209.
14. Rall W, Segev I (1987) in *Synaptic Function*, eds Edelman GE, Gall WF, Cowan WM (Wiley, New York), pp 605–637.
15. Goldberg J, Tamas G, Aronov D, Yuste R (2003) *Neuron* 40:807–821.
16. Soler-Llavina GJ, Sabatini BL (2006) *Nat Neurosci* 9:798–806.
17. Araya R, Jiang J, Eisenthal KB, Yuste R (2006) *Proc Natl Acad Sci USA* 103:17961–17966.
18. Diamond J, Gray EG, Yasargil GM (1970) in *Proceedings of the Fifth International Meeting of Neurobiologists*, eds Andersen P, Jansen J (Univ Forlaget, Oslo), pp 213–222.
19. Rall W (1964) in *Neural Theory and Modeling*, ed Reiss RF (Stanford Univ Press, Stanford, CA), pp 73–97.
20. Rall W, Burke R, Smith T, Nelson P, Frank K (1967) *J Neurophysiol* 30:1169–1193.
21. Yuste R, Urban R (2004) *J. Physiol (Paris)* 98:479–486.
22. Cash S, Yuste R (1998) *J Neurosci* 18:10–15.
23. Cash S, Yuste R (1999) *Neuron* 22:383–394.
24. Tamas G, Szabadics J, Somogyi P (2003) *J Neurosci* 22:740–747.
25. Leger J, Stern E, Aertsen A, Heck D (2005) *J Neurophysiol* 93:281–293.
26. Schiller J, Major G, Koester HJ, Schiller Y (2000) *Nature* 404:285–289.
27. Polsky A, Mel BW, Schiller J (2004) *Nat Neurosci* 7:621–627.
28. Holthoff K, Kovalchuk Y, Yuste R, Konnerth A (2004) *J. Physiol. (London)* 560:27–36.
29. Matsuzaki M, Ellis-Davies GC, Nemoto T, Miyashita Y, Iino M, Kasai H (2001) *Nat Neurosci* 4:1086–1092.
30. Ellis-Davies GCR (2003) *Methods Enzymol* 360A:226–238.
31. Majewska A, Yiu G, Yuste R (2000) *Pflügers Archiv Eur. J Physiol* 441:398–409.
32. Gasparini S, Magee J (2006) *J Neurosci* 26:2088–2100.
33. Losonczy A, Magee J (2006) *Neuron* 50:291–307.
34. Benavides-Piccione R, Ballesteros-Yañez I, DeFelipe J, Yuste R (2002) *J Neurocytol* 31:337–346.
35. Konur S, Rabinowitz D, Fenstermaker V, Yuste R (2003) *J Neurobiol* 56:95–112.
36. Andrasfalvy BK, Magee JC (2001) *J Neurosci* 21:9151–9159.
37. Holthoff K, Tsay D, Yuste R (2002) *Neuron* 33:425–437.
38. Rall W (1995) *The Theoretical Foundation of Dendritic Function* (MIT Press, Cambridge, MA).
39. Kalisman N, Silberberg G, Markram H (2005) *Proc Natl Acad Sci USA* 102:880–885.
40. Nuriya M, Jiang J, Nemet B, Eisenthal KB, Yuste R (2006) *Proc Natl Acad Sci USA* 103:786–790.
41. Elston GN, Benavides-Piccione R, DeFelipe J (2001) *J Neurosci* 21:RC163.
42. Larkman AU (1991) *J Comp Neurol* 306:332–343.
43. Heck D, Borst A, Antkowiak B (2003) *Neurosci Lett* 341:79–83.
44. Rall W, Segev I (1988) in *Computer Simulation in Brain Science*, ed Cotterill RMJ (Cambridge Univ Press, Cambridge, UK), pp 26–43.
45. Braitenberg V, Schüz A (1998) *Anatomy of the Cortex* (Springer, Berlin).
46. Nikolenko V, Nemet B, Yuste R (2003) *Methods* 30:3–5.
47. Hirase H, Nikolenko V, Goldberg JH, Yuste R (2002) *J Neurobiol* 51:237–247.